Numerical Study of Bubble Column Water-Air System by the VOF Method

GUESSAB AHMED
Department of Mechanical Engineering,
National Polytechnic School of Oran (Maurice Audin), Mechanical Manufacturing Technology,
Research Laboratory (LaRTFM-ENPO-MA),
Postbox 1523 EL-Mnaouer, Essenia Oran,
ALGERIA

Abstract: This paper aims to present a comprehensive study of the dynamics of a bubble using the Volume of Fluid (VOF) model in Fluent software. The simulation of two-phase flows is carried out by calculating the terminal velocity, bubble flow contours at different column heights, and the evolution of bubble circularity and Reynolds number at different times. The calculation was carried out on an air bubble with a diameter equal to 10 mm and zero introduction velocity by modifying the simulation parameters, such as the surface tension, to study their influence on the deformation of the bubble. This study will present four different shape regimes, which are obtained by varying the Bo (Bond number) and Mo (Morton number) values within the corresponding ranges of $1 < Bo < 10^3$ and $5\times10^{-8} < Mo < 10^2$. In addition, simulations are performed using large density and viscosity ratios of 1000 and 100, respectively. The results are comparable with great precision to the numerical simulation and experimental data.

Key-Words: - Air bubble, VOF, terminal velocity, Fluent, Bond number, Morton number.

Received: December 27, 2022. Revised: October 30, 2023. Accepted: November 26, 2023. Published: December 29, 2023.

1 Introduction

Bubble columns are used for different purposes because the process is simple to operate, has perfect mixing, has no moving parts and high mass transfer rates are achievable, along with the capability to accommodate a wide range of residence times by manipulating the gas and liquid flow rates, [1]. They are of particular interest for research. Despite the widespread applications of bubble columns, the interactions between hydrodynamics, mass transfer mechanisms, chemical reactions, and yield and product quality are to date poorly understood. Two-phase flows are ubiquitous in nature and industrial applications such as bioreactors, chemical industry, petrochemical, biochemical, metallurgical processes, solar energy, biogas energy nuclear engineering, etc. The physical mechanisms involved in these flows are fundamentally dependent on the separation surfaces between the different phases, which are called "interfaces". A moving bubble in a liquid medium deforms, which is of great interest. The problem of the rise of a bubble in a liquid at rest of infinite extension is complex because it involves very rich physics and coupled mechanisms.

The dynamics of a single bubble rising due to buoyancy in an infinite liquid pool have been the focus of many experimental, [2], [3], [4] and numerical studies, [5], [6], [7]. We can cite the terminal velocity and shape of the bubble, the trajectory of the bubble and its stability, and the deformations of the bubble during the ascent. In its simplest configuration, a bubble column consists of a vertically arranged cylindrical column filled with liquid. The gas flow rate is introduced at the bottom of the column through a gas distributor. The gas is supplied in the form of bubbles to either a liquid phase or a liquid-solid suspension. In this case, the solid particle size (typically a catalyst) ranges from 5 to 100 μm. These three-phase reactors are referred to as slurry bubble columns.

The liquid flow rate may be fed co-currently or counter-currently to the rising bubbles, or it may be zero. In the latter case, the column operates in batch condition. Bubble columns offer a significant number of advantages: excellent heat and mass transfer between the phases, low operating and maintenance costs due to the absence of moving parts, solids can be handled without any erosion or plugging problems, slow reactions can be carried out due to the high liquid residence time reasonable control of temperature when strongly exothermic reactions take place. However, the back-mixing of the liquid phase (the result of buoyancy-driven

recirculation) is a limitation for bubble columns: excessive back-mixing can limit the conversion efficiency. The reactor may be equipped with internals, baffles, or sieve plates, to overcome the back-mixing problem with an inevitable modification in the fluid dynamics. Bubble columns are extensively used in many industrial applications. They are of considerable interest in chemical processes involving reactions like oxidation, chlorination, alkylating, polymerization, and hydrogenation, as well as in the production of synthetic fuels via a gas conversion process (Fischer-Tropic process) in biochemical processes such as fermentation and biological wastewater treatment.

This study aims to simulate the formation of various air bubbles in stagnant water within a vertical column with a constant section. The study's findings could help us comprehend the actual physical phenomena and water column design. Lastly, it suggests novel standards for selecting mesh and geometry combinations that accurately depict the actual phenomena.

2 Geometry and Flow Configuration

The initial configuration for this numerical study corresponds to the study of the rise of an air bubble in the stagnant water. In this work, the single bubble diameter of D = 10 mm centred at (x, y) = (0.0056, 0) is studied. The dimensions of the column are a height of 100 mm and a width of 40 mm, as presented in Figure 1. The wall boundary condition is used at the top and bottom boundaries and for the two lateral borders. This bubble at an initial speed of zero and the ratios of density and viscosity are fixed. In our simulation, we assume that there is no phase change and that the fluids are Newtonian. In our work with these conditions, we can consider that the density and the viscosity of the gas (air) contained in the bubble have negligible effects compared to those of the surrounding liquid (water). The bubble is subject only to gravitational forces. The flow is controlled by two dimensionless numbers: the Bond number (Bo =10), and the Morton number (Mo = 5×10^{-6}). The parameters of the numerical simulation are chosen to obtain the same Bond and Morton number values as in some of the reference simulation, [8] and experiments, [9]. In this work, the primary phase is water (liquid) and the secondary phase is air (gas). The main physical properties are used to observe and describe the matter of the single air and water is tabulated in Table 1.

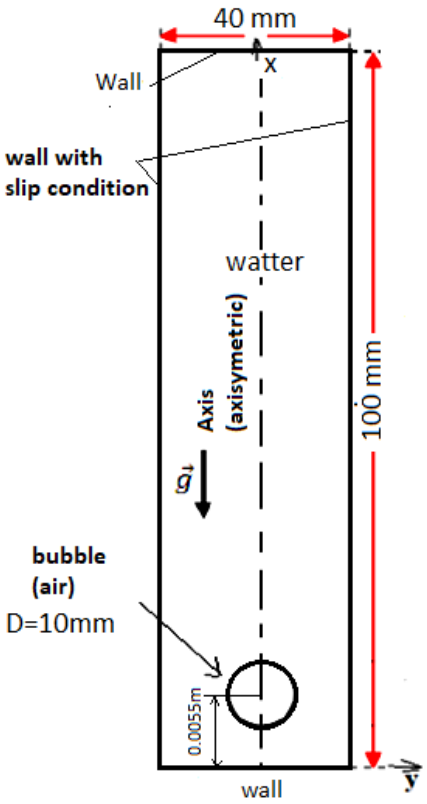

Fig. 1: Schematic of column geometry with Initial configuration of bubble

Table 1. Simulation parameters, [8]

Time scale	$\sqrt{D/g}$
Nature of simulation	2D-Axisy.
Regime	Laminar
Unsteady time step	CFL< 0.25
Density of the liquid, ρ_l	1000 [Kg.m^{-3}]
Air bubble density, ρ_g	1 [Kg.m^{-3}]
Liquid dyn. Viscosity, μ_l	0.0266[Kg/m.s]]
Air Dyn. viscosity, μ_g	0.000266[kg/m.s]
Interracial tension, σ	0.1[N.m^{-1}]
Gravity, g	10 [m.s^{-2}]
Bubble diameter, D	0.01m
Morton's number, Mo $Mo=\left(g\mu_l^4\right)/\left(\rho_l\sigma^3\right)$	5×10^{-6}
Number of Bond, Bo $Bo=\rho_l gD^2/\sigma$	10
Density ratio ρ_l/ρ_g	1000
Viscosity ratio μ_l/μ_g	100

3 Governing Equations

If we assume that the movement of each of the phases that make up the flow obeys the incompressible Navier-Stokes equations, it is possible to show that, under certain hypotheses, [10], the evolution of two-phase mixing can be

described on the à scale by the system of Navier-Stokes equations:

$$\frac{\partial V}{\partial t}+\nabla.(V.V)=-\frac{1}{\rho}\nabla P+g+\frac{1}{\rho}\nabla.\left[\mu\left(\nabla.V+\nabla^{t}V\right)\right] \quad (1)$$
$$-\frac{\sigma}{\rho}(\nabla.n)$$

$$\nabla.V=0 \quad (2)$$

Where P is the pressure, V is the velocity, g is the gravity, σ is the interfacial tension, ρ and μ denoting for example the mass volume and the local dynamic viscosity of the mixture. In this bubble simulation, $-\frac{\sigma}{\rho}\left(\nabla.\vec{n}\right)$ represents the volumetric forces at the interface resulting from the surface tension force per unit volume. Where σ the coefficient of surface tension and n is the surface normal which is estimated from the gradient of volume fraction, $-\left(\nabla.\vec{n}\right)$ is the local surface curvature calculated as follows:

$$-(\nabla.\hat{n})=\frac{1}{n}\left[\frac{n}{|n|}\nabla|n|-(\nabla.n)\right] \quad (3)$$

To arrive at equation (1), it is in particular necessary (a) to assume the absence of phase change and (b) to neglect the local deviations between the point values of the different quantities. The last equation constituting the model is:

$$\frac{\partial C}{\partial t}+V.(\nabla.C)=0 \quad (4)$$

The flow of two fluids is represented by a model with a single fluid that remains incompressible but, whose density and physical properties vary strongly when crossing the interfaces. The density and viscosity of the fluid are expressed, as a function of the properties of the two fluids (gas/liquid) and of the volume fraction C of one of the phases, as follows:

$$\rho=C.\rho_1+(1-C)\rho_2 \quad (5)$$
$$\mu=C.\mu_1+(1-C)\mu_2 \quad (6)$$

3.1 The VOF Method

The CFD Fluent code has a variety of models available to incorporate multiphase flow. The FLUENT, [11], code was utilized to solve the transport equations for two-phase flow, and the liquid-gas interface was monitored through the Volume of Fluid (VOF) method. The VOF method uses a discrete function $C=f(x,y,t)$ that represents the volume fraction of one of the fluids in each control volume. For $C=1$ and $C=0$, the cell represents the vapor region (in bubble) and the water region (in liquid fluid), respectively. And for $0<C<1$, the cell represents the interface region. The free surface of the bubble exists in the interface region. In this study, the bubble is defined as an aggregate composed of cells that have a volume fraction in the range of $C>0.5$. Therefore, the bubble volume is calculated by the summation of the vapor volume in each cell where the volume fraction is in the range of. And bubble surface area is calculated using the area of iso-surface which has a constant volume fraction. Figure 2 shows the governing equations in each cell, governing equations (Eq. 1 and Eq. 4) are solved for only gas and liquid phases, respectively. However, in the interface cell, governing equations are solved for the mixture phase assumed as 3rd phase.

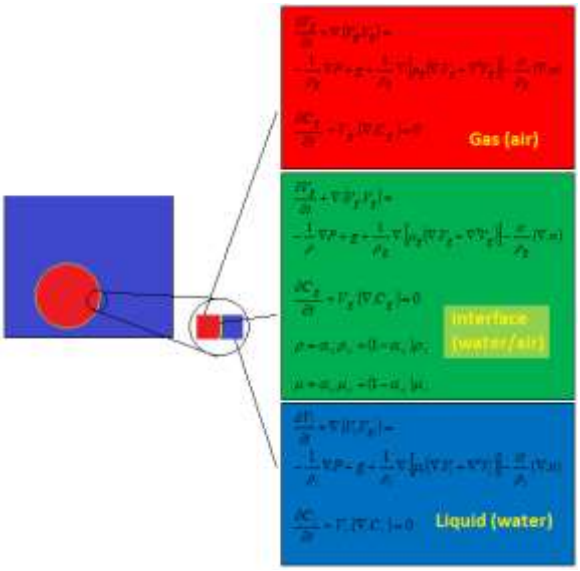

Fig. 2: Governing equation in each cell

The flow of the two fluids is represented by a model with a single fluid that remains incompressible, but whose density and physical properties vary strongly when crossing the interfaces. In various applications of multiphase flows, a fundamental understanding of the physics of the case of a bubble rising and deforming in a quiescent viscous liquid is essential. Herein, the bubble shapes tend to vary greatly, depending on where the bubbles lie within the different flow regimes. The bubble-rising behaviors can usually be correlated against four non-dimensional parameters such as the Morton number which is defined as:

Bond number: $Bo=\frac{g\Delta\rho D^{2}}{\sigma}$ (7)

Morton number: $Mo = \frac{g\Delta\rho\eta_l^4}{\sigma^3\rho_l^2}$ (8)

Where, $\Delta\rho = \rho_l - \rho_g$

Bo is the ratio of the body forces (effective gravitational forces) and the surface tension, but it could also be considered as a dimensionless size value of the bubble. *Mo* describes the properties of the surrounding fluid, mainly focusing on viscosity and surface tension.

The Froud number is defined as:

$$Fr = \frac{U_0^2}{gd_0} \quad (9)$$

And the Reynolds number is defined as:

$$\mathrm{Re} = \frac{\rho_l UD}{\mu_l} \quad (10)$$

Where, D and d_0, represent the diameter of the bubble and orifice diameter, respectively. The Bond number represents the contribution of the effects of surface tension and buoyancy, whereas the Morton number, which is sometimes referred to as the property group, measures the relative importance of viscosity and surface tension forces. Following a similar definition, the Reynolds number signifies the contribution between the inertia and viscous effects.

3.2 Numerical Method

Before being able to launch a numerical simulation, it is necessary to carry out several steps, including the construction of the geometry of the system and its spatial discretization (mesh), the choice of adequate boundary conditions, and the initial conditions. A two-dimensional uniformly structured mesh is developed using GAMBIT, [12].

The mesh is shown in Figure 3. The domain presented in this figure is meshed into quad elements. The boundary conditions are symmetry on the axis (Ox) and walls on the horizontal and vertical boundaries (Figure 1). The time step was set to 10^{-4}s. The initial position of the bubble is shown in Figure 3.

The numerical simulation of a dynamic bubble is carried out using Fluent. The geometries used are of the two-dimensional asymmetric type. The governing equations are solved using an incompressible approach (pressure-based solver) in the simulations for a water-air two-phase flow system. Water and air were selected as the primary and secondary phases, respectively. The simulations are carried out in the bubbly laminar unsteady regime. The finite volume method with an implicit scheme for iterations was used to solve the continuity, momentum, and volume fraction equations. The first-order scheme (upwind) was applied to the discretization of the flow equations (Navier-Stokes equations) and the volume fraction. The pressure-velocity coupling was carried out using the implicit scheme with the SIMPLE method and the discretization of the pressure using the Standard scheme. The convergence criterion is set to 10^{-4} for all equations. For the unsteady case, it is necessary to choose and adapt the time step for each case of the simulation.

The standard Current-Friedrich-Lewy (CFL) number should ideally be kept below 0.25. Its value is reported in the fluent window. This Currant number is roughly the number of cells that converted information travels at the speed of the bubble in one time step:

$$CFL = \frac{V(t).Dt}{Dx} \quad (11)$$

Thus, it is from the terminal velocity noted in Figures 11, Figure 12, Figure 13, and Figure 14, and in order to ensure a CFL= 0.25 the time step proposed in Table 3 was calculated.

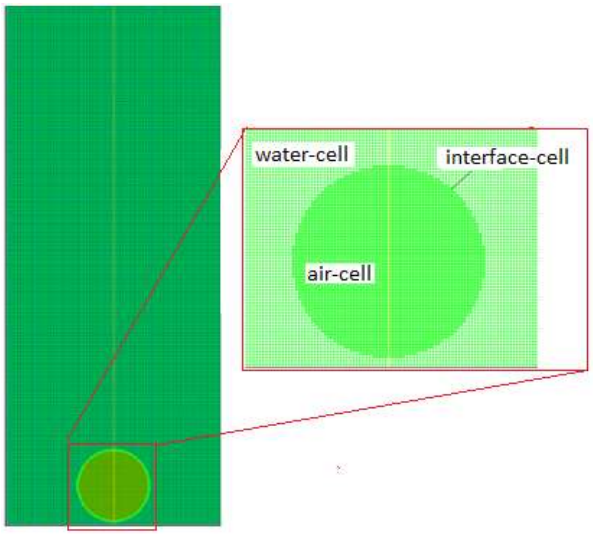

Fig. 3: A view of the bubble mesh in the middle of the column and around the bubble

4 Results and Discussions

The results of air bubbles rising in water will be examined here and compared to numerical, [8] and experimental data, [9]. To be able to study the temporal evolution of the bubble speed in the vertical direction along the axis (Ox), it is necessary to calculate for each time step (t), the average axial speed (V (t): barycentric speed of the bubble) defined as:

$$V(t)=\frac{\int_{\vartheta} C(x,t)V(x,t)d\vartheta}{\int_{\vartheta} C(x,t)d\vartheta} \quad (12)$$

In practice, we determine the Bond number (Bo) and the Morton number (Mo) and calculate the Reynolds number Re (t) using the simulation results.

$$\mathrm{Re}(t)=\frac{\rho_l V(t)D}{\mu_l} \quad (13)$$

The first step is to determine the minimum number of calculation cells needed per initial bubble diameter to accurately describe its dynamics. To quantify this number, a bubble rise simulation is made for different spatial resolutions of grid1 ($\Delta x = \Delta y = d/50$), grid2 ($\Delta x = \Delta y = d/70$) and grid3 ($\Delta x = \Delta y = d/90$). The Reynolds number is compared for the different spatial resolutions in Figure 4. The terminal velocity converges to a single curve as the resolution increases. It has been observed that the terminal velocity of the bubble obtained from x = d/50 is only 5% lower than that obtained from x = d/90.

In addition, there is a good correspondence between the numerical simulation and the experimental one, [8] and [9], the comparison of the temporal evolution of the speed of the bubble that we obtain shows a great resemblance. The results indicate that 50 computational cells per initial bubble diameter is an acceptable lower limit for accurately describing bubble dynamics in the regime considered here. In terms of terminal velocity, we obtain a Reynolds number of 96.5 very close to that found by, [8] (Re = 100) and Re = 98.53 by simulation, [9].

The deformation of the bubble in the fluid is determined by its acceleration. It appears when observing Figure 3 that the speed increases and reaches a maximum to return to its asymptotic speed, and we then notice that the speed has increased and will eventually stabilize. In other words, the bubble returns to its constant shape once the speed is stabilized.

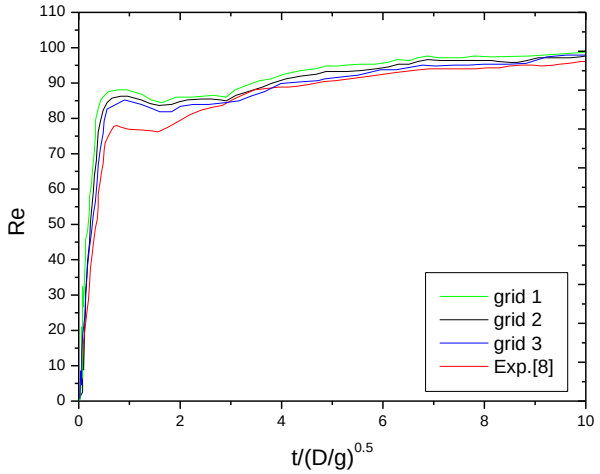

Fig. 4: Reynolds number (mean velocity) profile in different meshes

That is to say, the bubble recovers its constant shape when the speed is stabilized. After having obtained the correct settings under Fluent, we will now proceed to the analysis of the results of the simulation. The procedure we use is similar to that of an experimenter. We therefore release a spherical air bubble with a diameter of 0.01 m and zero initial velocity in the water at rest. Figure 5a shows the evolution of the shape of the bubble over time. Under the effect of Archimedes' force, the bubble begins to rise and deform before acquiring its terminal speed and shape. The terminal shape we end up with is very similar to that obtained by, [9], by simulation (Figure 5b). In the first stage, the bubble widens at the back and the curvature becomes negative in this region. Then, still at the back, the curvature decreases, vanishes, and then becomes positive again. In the third stage, the part located near the intersection of the base and the upper dome rises. The bubble then changes from a spherical cap shape to a quasi-ellipsoidal shape close to front-back symmetry. In a last time, the front part flattens while the rear part hardly evolves anymore. This same evolution of the shape of the air bubble is observed by Blanco. It can be said that the back of the air bubble deforms more than the front because gravity and capillary forces combine. After having observed and compared the evaluation of the bubble, we can take an interest in its circularity. Its evolution is then traced (Figure 6). We then observe a sudden drop in the circularity of the bubble, which deforms during its ascent and then ends up stabilizing and reaching a constant value. We can therefore think that this reduction in circularity is caused by the acceleration of the bubble in the water, which deforms it.

To confirm this hypothesis, we then plot the rate of ascent of the bubble as a function of time.

Vectors may be used to illustrate how the velocity field impacts the bubble, as seen in Figure 7. The arrows represent the velocity field of the flow, which is colored according to the vorticity of the flow. By observing this figure, we see that the flow around the air bubble creates an acceleration of the fluid at the lateral ends, causing the creation of a vortex at the interface. These vortices then deform the bubble, thus creating a drop in the circularity of the bubble.

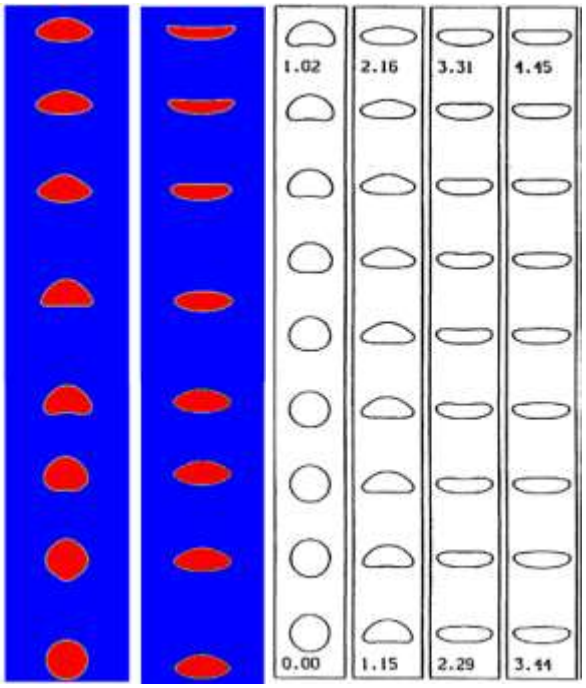

(a) (b)

Fig. 5: A two-dimensional air bubble rising in a low-viscosity liquid ($\rho_l / \rho_g = 10^3$, $\mu_l / \mu_g = 10^2$, Mo=10, Bo=5×10^{-6}). (a) Simulation, (b) Experiments, [9].

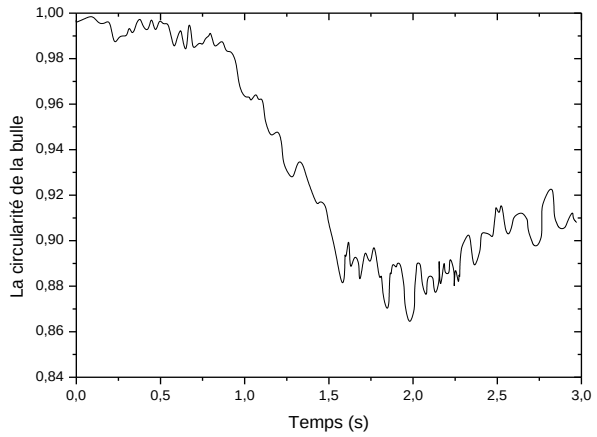

Fig. 6: Evolution of bubble circularity (case: Bo=10, Mo=5×10^{-6}, σ=1.0)

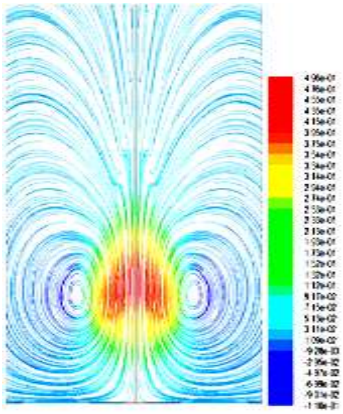

Fig. 7: Representation of the axial velocity field around the bubble in red (time = 0.032 s)

One can also observe the evolution of the streamlines in a frame linked to the air bubble in Figure 8. The shape of the bubble not only influences its terminal ascent velocity but also plays an important role in determining the rate of heat and mass transfer. We notice in Figure 5 that, following their moving interface, the bubbles deform when they undergo external flow fields until there is equilibrium between the normal and shear stresses at the interface. Generally speaking, the shapes observed during the rise of the air bubble in the following figure can be divided mainly into two categories. At the beginning of the evolution, the shape of the bubble is spherical, and for a certain moment, the air bubble deforms and takes on an ellipsoidal form. The shape of the bubble is flattened with a convex interface (seen from the inside). We can conclude that the forces of surface tension and viscosity, which are dominant in this research configuration, are responsible for the shape change of the bubble. The interface of the bubble can be considered rigid; it plays the role of a membrane, and the movement of the bubble is purely vertical. This part deals with the case of bubbles deforming a lot but evolving at Reynolds numbers of the order of ten and the case of bubbles that deform little but for which the Reynolds number is of the order of a hundred. To compare our results with those of, [8], and, [13], we conducted a series of simulations in a range of Morton numbers (5×10^{-8}, 5×10^{-6}, 10, and 10^4) and a Bond number range (1, 10, 100 and 1000). This corresponds a posterior to a Reynolds number range Re = 10 and 100. Now let's look at how the surface tension of the water/air fluid affects the air bubble's rising dynamics.

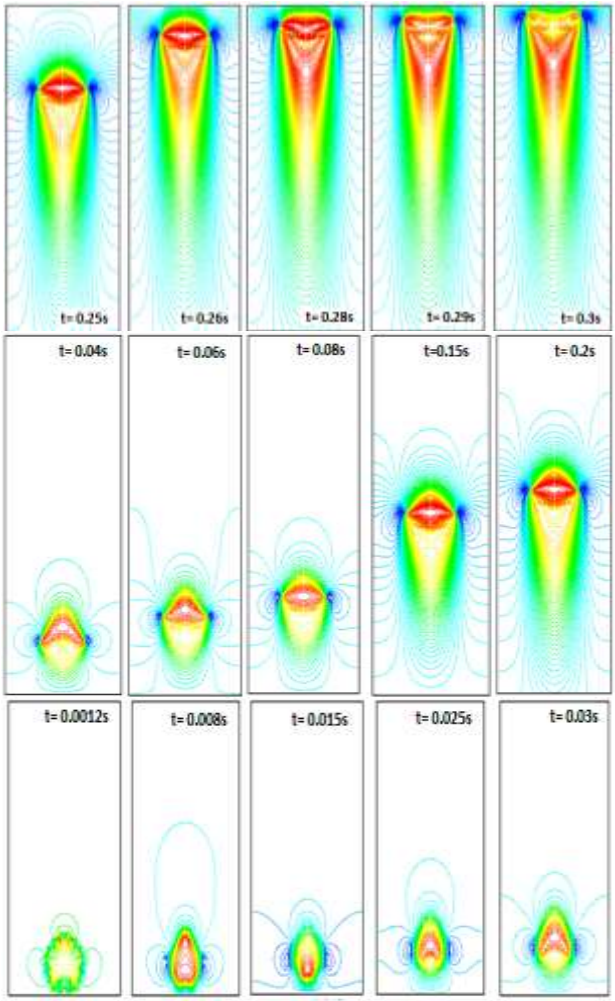

Fig. 8: The vertical axial velocity field of the bubble refers to a frame moving with the bubble

To do this, we fix ρ_l/ρ_g and μ_l/μ_g (1000, 100), respectively, and we choose four pairs of values (Bo, Mo). Table 2 shows the combinations to choose among the values of viscosity, surface tension, and the corresponding time step for the simulation. We note that the validation of our numerical simulation is based on the shape map developed by, [13]. These shape maps show the shape of bubbles for most conditions of practical interest and are based on dimensionless numbers (Re, Mo, and Bo); Figure 9.

Table 2. Parameters for the simulation
(All in S.I. units)

case	1	2	3	4
μ_l	0.04729	0.0266	0.1778	0.05623
σ	1	0.1	0.01	0.001
Δt	1×10^{-4}	1×10^{-4}	2×10^{-4}	5×10^{-4}
Mo	5×10^{-8}	5×10^{-6}	10	10^2
Bo	1	10	10^2	10^3

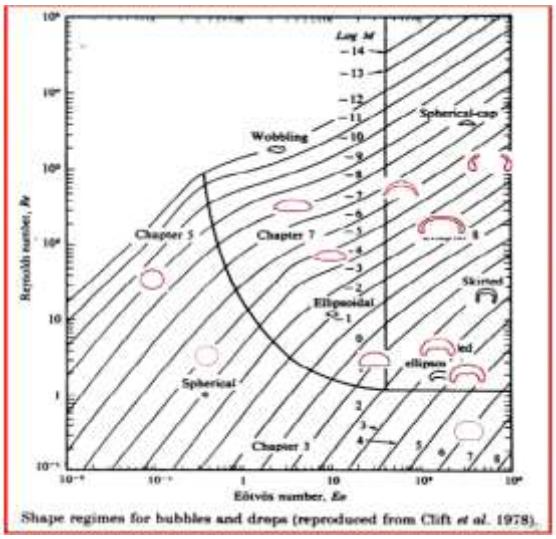

Fig. 9: Bubble regimes, according to, [13].

The four series of Figures 9a, 9b, 9c, and 9d make it possible to appreciate the decisive influence of the tension of the surface between the two fluids (water and air) on the rise time of the bubble. The first remark that can be drawn from these figures is that a low surface tension 'σ' allows a greater deformation of the bubbles. The shape of the bubble not only influences its terminal ascent velocity but also plays an important role in determining the rates of heat and mass transfer. According to these figures, the bubbles deform when they experience external flow fields until there is equilibrium between the normal stress and the shear stress at the interface. Bubble shapes are limited in number due to interfacial forces. The observed forms of rising bubbles in our numerical simulation using the VOF method fall primarily into three groups.

- Spherical bubbles: at stationary Reynolds number Re = 100 and surface tension σ= 1.0 N/m^2. Note that surface tension forces and viscous forces govern the shape of the bubbles, which deviate very little from the spherical shape; see the bubble shape of our simulation in Figure 10a and the experimental in Figure 9.
- Ellipsoidal Bubble (Ellipsoidal): As shown in Figure 10b, ellipsoidal bubbles are defined as bubbles that have flattened and a convex interface encircling the entire surface. These bubbles undergo periodic expansion or rotational movement.
- The spherical cap bubble or ellipsoidal cap (Dimpled ellipsoidal cap): bubbles (Figure 10c); these bubbles look like segments cut from the spheres by both sides of the bubble.

- For the case σ=1 [N/m^2] (Figure 10d), the rising bubble in a Newtonian fluid behaves like a rigid sphere and follows Stokes' law in its motion.

The terminal velocities of ascent for the four bubbles as a function of time are shown in Figure 11, Figure 12, Figure 13 and Figure 14. These figures show that the Reynolds number of the bubble plays an important role, i.e., with an increase in these values, the bubble will change from one shape to another. The time course of the Reynolds number of the four bubbles in cases 1 to 4 shown in Figure 11, Figure 12, Figure 13 and Figure 14 is quite different because the repulsive irrotational effect acts in region $t/(D/g)^{0.5} < 3$.

Table 3 compares the Reynolds number in the stationary case of the air bubble rising in a water column between our simulation study and that of, [8].

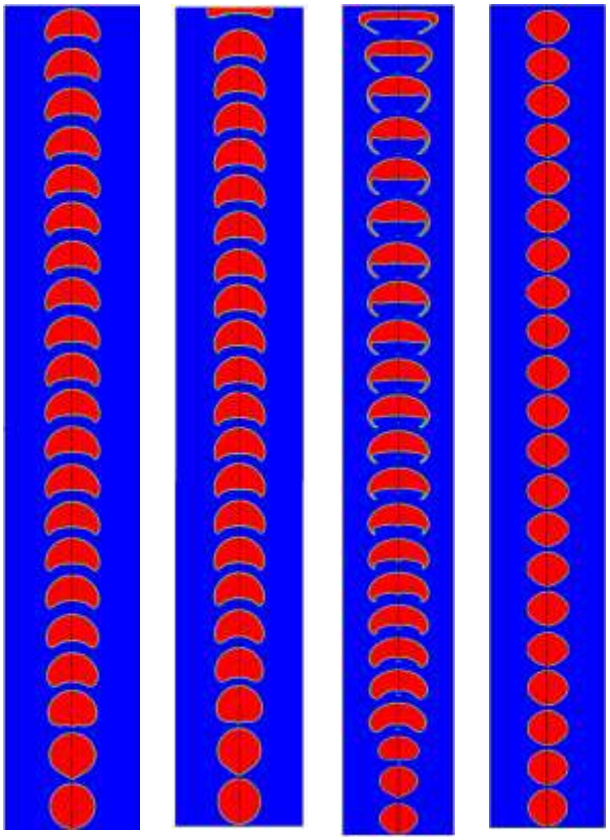

σ =0.1 [N.m^{-2}] (a) σ =0.01 [N.m^{-2}] (b) σ =0.001 [N/m^2] (c) σ =1.0 [N.m^{-2}] (d)

Fig. 10: Simulation results of the single bubble with a 10 mm diameter rising at four different configurations (σ = 0.1, 10^{-2}, 10^{-3}, and 1.0 [N.m^{-2}])

Table 3. Comparison of Reynolds number with the reference

case	(a)	(b)	(c)	(d)
σ =	0.1	0.01	0.001	1
Simulation	96.55	94.34	9.22	96.56
Exp. [8]	98.53	95.61	9.56	98.64

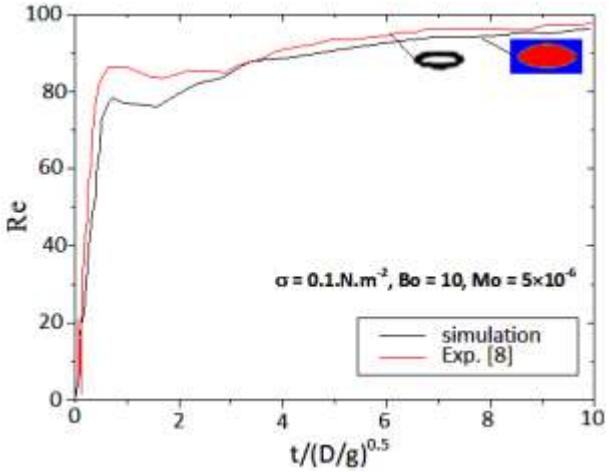

Fig. 11: Time history of the Reynolds number of bubbles (case: Bo=10 and Mo=5×10^{-6})

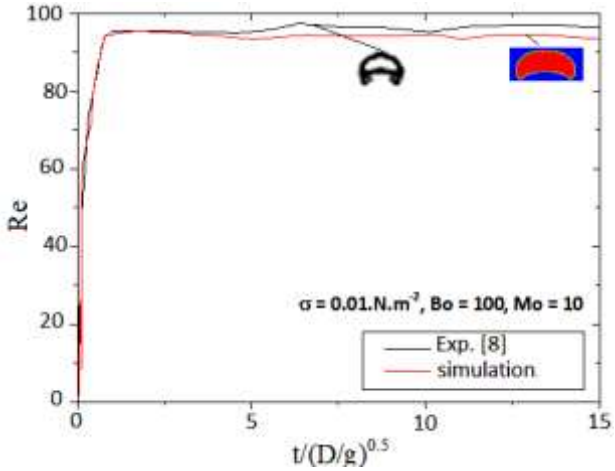

Fig. 12: Time history of the Reynolds number of bubbles (case: Bo=100 and Mo=10)

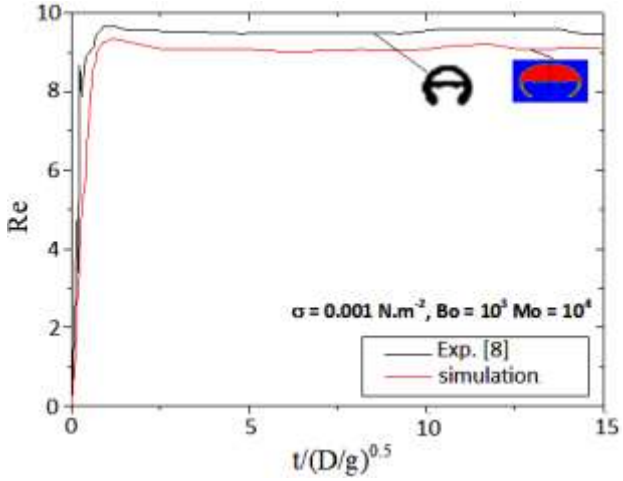

Fig. 13: Time history of the Reynolds number of the bubble (case: Bo=10^3 and Mo=10^4)

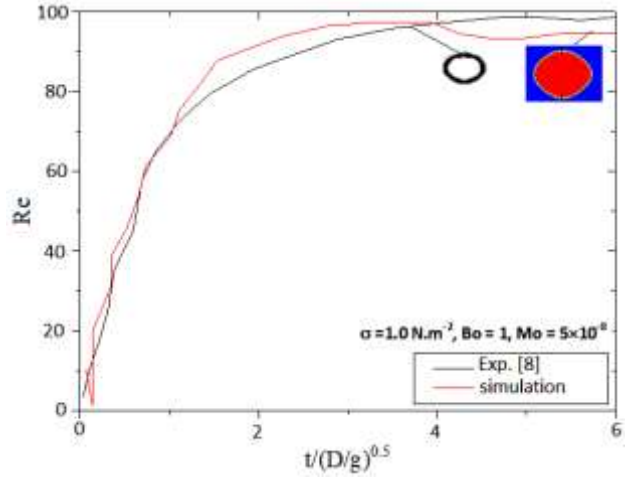

Fig. 14: Time history of the Reynolds number of the bubble (case: Bo=1 and Mo=5×10^{-8})

5 Conclusion

A CFD simulation of the hydrodynamics of a gas-liquid bubble column has been simulated using Fluent by employing the VOF approach. We can conclude that in a viscous fluid (water), the bubbles go through well-known shapes: spherical shape, ellipsoid of revolution crushed vertically, flattening of the rear part of the bubble until obtaining, for larger volumes, a helmet-shaped spherical shape. This helmet or spherical cap flattens as the volume of the bubble increases. In the fluid Newtonian, whatever their size, the bubbles do not have a tail but present, from a certain volume, the shape of a parachute like a depression at the back of the bubble.

Our numerical validation was concluded for a series of rising bubbles, in a stagnant fluid. We obtained a good agreement with the experimental data available from, [9]. The objectives of this study are:

- Integrating the VOF approach with a computation code (FLUENT) and evaluating the output CFD scheme's performance against several experimental and numerical examples;
- Use our algorithm to create a new computer model that simulates the VOF method;
- A column with a constant vertical section can be used to simulate the rising dynamics of a bubble. For this, a variety of validations of the resulting model will then be carried out in the form of test cases;
- Work with the UDF to change an important commercial code to meet our study goals.

This work remains a modest contribution to the field of understanding phenomena and the characterization of the physical parameters linked to the bubble. For our future research, we can cite some perspectives that it would be interesting to develop, among which we cite some:

1. The impact of temperature on the bubble's dynamics;
2. An examination of the necessary development of the heat transfer model, which takes into account the microlayer region underneath the bubble
3. Examining the three-dimensional movement of bubbles using fluid code.

Acknowledgements:
The author would like to thank the anonymous reviewers and the editor for their insightful suggestions.

References:

[1] Ghasem N., Mass transfer modeling in nanofluids: theoretical basics and model development. In *Nanofluids and Mass Transfer*, pp.247-271. Elsevier 2021.

[2] Li Mei, Xiaopeng Chen, Bei Liu, Zhongyao Zhang, Tingting Hu, Jiezhen Liang, Xiaojie Wei, and Linlin Wang, Experimental Study on Bubble Dynamics and Mass Transfer Characteristics of Coaxial Bubble in Petroleum-Based Liquids, *ACS Omega*, Vol.8, No.19, 2023, pp. 17159-17170.

[3] Q. Feng, Q. Wang and C.Y. Zhao, Experimental Study on Three-Dimensional

Bubble Rising Behaviours by Virtual Stereo Vision. *Journal of Applied Fluid Mechanics,* Vol. 16, No. 4, 2023, pp. 805-818.

[4] Liu, Y.; Upchurch, E.R; Ozbayoglu, E.M, Experimental Study of Single Taylor Bubble Rising in Stagnant and Downward Flowing Non-Newtonian Fluids in Inclined Pipes, *Energies*, Vol. 14, No 3, 2021, pp. 578.

[5] Corina B., Lăcrămioara D. R., Study of air bubble dynamics in an air column using CFD, *E3S Web of Conferences* Vol. 85, 2019, pp. 4-5.

[6] Hussein E. Q., F. L. Rashid, A. K. Hussein and O. Younis, Hydrodynamics of Single Bubble Rising Through Water Column using Volume of Fluid (VOF) Method, *Journal of Thermal Engineering,* Vol. 7, No. 14, 2021, pp. 2107-2114.

[7] Narjes K., M. Karamoozian and H. Nour-Bidgoli, An investigation of the effect of initial bubble diameter on the bubble trajectory in the flotation column cell using CFD simulation, *The Mining-Geology-Petroleum Engineering Bulletin,* Vol. 37 No. 2, 2022, pp. 1-12.

[8] T. Bonometti, J. Magnaudet, An interface-capturing method for incompressible two-phase flows. Validation and application to bubble dynamics. *International Journal of Multiphase Flow,* Vol. 33, No. 2, 2002, pp.109-133.

[9] Blanco A. A., Some Aspect of the Flow of a Viscous Fluid Around a Deformable Bubble. An Analysis by direct Simulation. Thesis of The Natioanl Polytechnic Institute of Toulouse, Fluid Mechanics Speciality, Toulouse IMFT (1995), France.

[10] C. W. Hirt, B. D. Nichols, Volume of Fluid (VOF) Method for the Dynamics of Free Boundaries. *Journal of Computational Physics* Vol. 39, No. 1, 1981, pp. 201-225.

[11] ANSYS Inc, 16.3 Volume of Fluid (VOF) Model Theory, 2009, [Online]. https://www.afs.enea.it/project/neptunius/docs/fluent/html/th/node297.htm (Accesses Date: December 23).

[12] GAMBIT, Tutorial Guide, September 2004, [Online]. https://wp.kntu.ac.ir/mojra/CFD-gambit22tutorial.pdf (Accesses Date: December 23)

[13] Clift, R., Grace, J.R., Weber, M.E., *Bubbles ,drops and particles*. Academic Press, Inc., New York, 1978.

Contribution of Individual Authors to the Creation of a Scientific Article (Ghostwriting Policy)

GUESSAB Ahmed carried out the simulation, interpretation (discussion), and verification of results.

Sources of Funding for Research Presented in a Scientific Article or Scientific Article Itself

Research funded by the Mechanical Manufacturing Technology Research Laboratory (LaRTFM-ENPO-MA)

Conflict of Interest

The author declared no potential conflicts of interest with respect to the research, authorship, and/or publication of this article.